Available online at www.sciencedirect.com

ScienceDirect

Ceramics International 40 (2014) 2295–2298

CERAMICS INTERNATIONAL

www.elsevier.com/locate/ceramint

Hydrothermal synthesis and gas-sensing properties of ultrathin hexagonal ZnO nanosheets

Weiwei Guo[a,*], Min Fu[a], Chongzhi Zhai[b], Zhongchang Wang[c,**]

[a]*Chongqing Key Laboratory of Urban Atmospheric Environment Comprehensive Observation and Pollution Prevention and Control, College of Environmental and Biological Engineering, Chongqing Technology and Business University, Chongqing 400067, PR China*

[b]*Chongqing Environmental Science Research Institute, Chongqing 400067, PR China*

[c]*WPI Research Center, Advanced Institute for Materials Research, Tohoku University, 2-1-1 Katahira, Aoba-ku, Sendai 980-8577, Japan*

Received 24 July 2013; received in revised form 30 July 2013; accepted 30 July 2013
Available online 11 August 2013

Abstract

Gas-sensing performances are often enhanced significantly once size of the sensing materials approaches a critical value of 15 nm. Here, we synthesize, by a simple hydrothermal method, ultrathin hexagonal ZnO nanosheets with a thickness of 17 nm. The cetyltrimethylammonium bromide is found to play a critical role in producing such unique hexagonal ZnO nanosheets, and a possible growth mechanism is proposed. The as-prepared ultrathin nanosheets exhibit excellent gas-sensing properties to formaldehyde gas at optimal temperature of 350 °C under concentration of 50 ppm, rendering the ultrathin nanosheets promising for the on-site detection of formaldehyde.

Keywords: D. ZnO; Crystal growth; Nanosheet; Formaldehyde; Gas sensors

1. Introduction

Zinc oxide (ZnO), as a functional *n*-type semiconductor, has already been utilized as a gas-sensing material for detecting toxic or hazardous gases because of its typical properties, such as insusceptible resistivity, high electrochemical stability, nontoxicity, and abundance in nature [1]. Recent studies have demonstrated that morphology has a significant influence on gas-sensing properties of nanomaterials [2–5]. For example, one-dimensional (1D) structures of ZnO, such as nanowires [6], nanorods [7] and nanobelts [8], and their hierarchical structures have been widely used for gas sensors [9,10]. In addition, two-dimensional (2D) structures of ZnO, such as nanoplates, can also often be fabricated [1,11]. To date, most work has been reported on sheet-based 3D-structured ZnO gas sensors or thick-sheet ZnO gas sensors [12,13]. However, few works have been conducted on the gas sensors made of polygonal nanoflakes.

Notwithstanding these intensive researches, the key factors governing gas-sensing properties of ZnO remain under debate. One consensus is that size and morphology of gas-sensing materials shall often play an important role in enhancing a series of gas-sensing performances. For instance, Xu et al. [14] reported that gas sensitivity of SnO_2 can be improved significantly once its size falls below ~10 nm. This has been confirmed by Yamazoe et al. claiming that the critical size of SnO_2 nanomaterials is 5–15 nm for an effective detection of H_2 and CO [15]. Although Hongsith et al. [16] recently proposed a new general concept to address adsorption mechanism of the ZnO nanostructures to ethanol gas, they still attributed the pronounced enhancement of the sensing responses to the small size of ZnO nanomaterials (~15 nm). In this work, we demonstrate a successful synthesis of thin hexagonal ZnO nanosheets *via* a facile and economical hydrothermal process. The crystallinity, morphology, and microstructure of the prepared nanosheets are investigated, based upon which the likely formation mechanism is discussed. The prepared hexagonal ZnO nanosheets are found to exhibit good gas-sensing performances to the formaldehyde gas.

2. Experimental

All chemical reagents were of analytical grade and used with no further purification. The zinc acetate dehydrate (Zn

*Corresponding author.
**Corresponding author. Tel.: +81 22 217 5933,+81 22 217 5930.
E-mail addresses: shendaguowei@163.com (W. Guo), zcwang@wpi-aimr.tohoku.ac.jp (Z. Wang).

0272-8842/$ - see front matter © 2013 Elsevier Ltd and Techna Group S.r.l. All rights reserved.
http://dx.doi.org/10.1016/j.ceramint.2013.07.150

$(CH_3COOH)_2 \cdot 2H_2O)$ (1 mM), and hexamethylene tetramine (HMT) (0.5 mM) and cetyltrimethylammonium bromide (CTAB) (0.05 g) were first dissolved into distilled water (40 mL), followed by strong stirring for 1 h using magnetic stirrer. The solution was then transferred into autoclaves which were heated to 120 °C and maintained for 12 h. Finally, the white products were harvested by pursuing centrifugation, washing with distilled water and ethanol to remove unexpected ions, and drying at 60 °C in air.

Microstructural analysis was conducted by the x-ray diffraction (XRD), scanning electron microscopy (SEM), and transmission electron microscopy (TEM). For the XRD, a Rigaku D/Max-1200X diffractometry with Cu $K\alpha$ radiation operated at 40 kV and 200 mA was applied. Surface morphologies of the samples were observed using a Hitachi S-4300 SEM. Microstructure and chemical composition were further analyzed using the JEOL JEM-2010F electron microscope operated at an accelerating voltage of 200 kV. Gas sensors were fabricated by first dispersing the prepared ZnO powders in distilled water and then making pastes via ultrasonication. The pastes were next coated onto an alumina ceramic tube and the thickness of the pasted films spans the range from 0.5 to 1 mm. Response of the sensors (S) was defined as the ratio of their resistances in air (R_a) to those in target gases (R_g) [9]. Response and recovery time was defined as the time taken by the sensors to achieve 90% of total resistance change during either the adsorption or the desorption process.

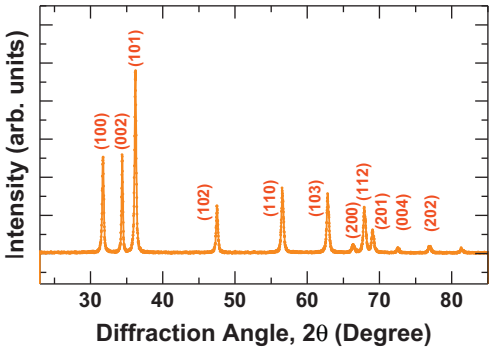

Fig. 1. XRD spectra of the ZnO hexagonal nanosheets.

3. Results and discussion

3.1. Microstructural characterization

Fig. 1 shows typical XRD patterns of the as-prepared ZnO. The hexagonal phase with lattice constants of $a=3.256$ Å and $c=5.212$ Å was detected for ZnO with no clear evidence of impurities, indicating that all as-prepared products are pure wurtzite ZnO, regardless of the surfactants. In addition, we also note several strong and sharp diffraction peaks, which indicates that the as-prepared ZnO are highly crystallized yet polycrystalline.

Fig. 2(a)–(f) shows the representative SEM and TEM images of the as-prepared products. From Fig. 2(a), the as-synthesized ZnO product presents uniform hexagonal nanosheets and it is obvious that these nanosheets are not aggregated in spite of their quite small size and ultrathin layer. An enlarged SEM image of an individual hexagonal nanosheet is shown in Fig. 1(b) and (c), from which the thickness and side length of these perfect hexagonal nanosheets are determined to be approximately 17 and 90 nm. Fig. 2(d) shows TEM image of a perfect hexagonal nanosheets. A clear white and black background is seen, which indicates that the

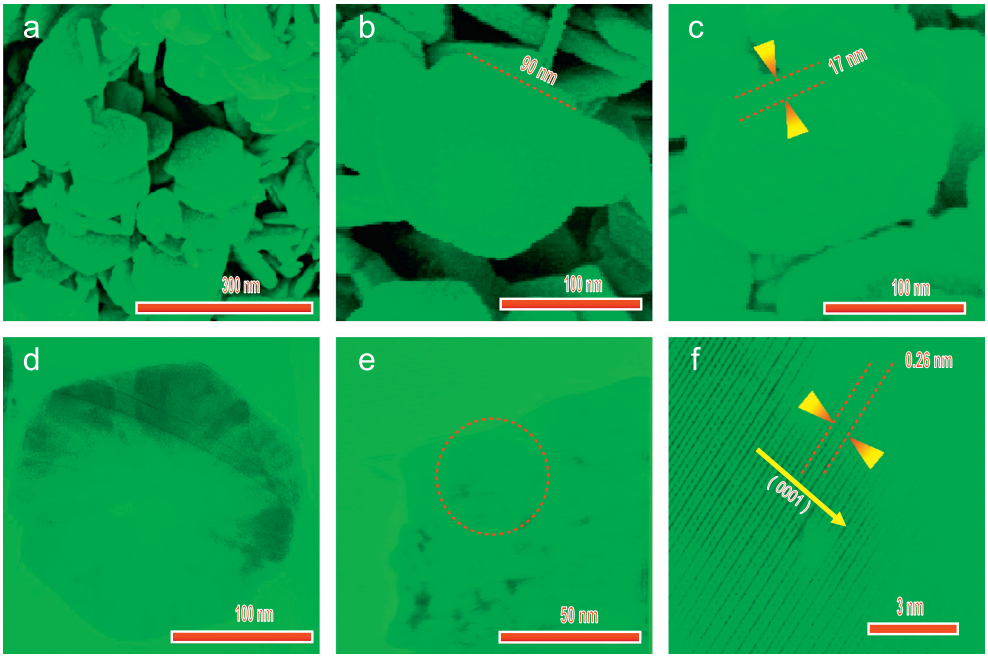

Fig. 2. (a–c) SEM images of the ZnO hexagonal nanosheets. (d–f) TEM images of the ZnO hexagonal nanosheets. (For interpretation of the references to color in this figure, the reader is referred to the web version of this article.)

hexagonal nanosheet is indeed very thin. Fig. 2(e) shows TEM images of edge regions of the hexagonal ZnO nanosheet, showing unambiguously that the nanosheet is assembled by nanoparticles. Fig. 2(f) presents a high-resolution TEM (HRTEM) image of the nanoparticle (marked with red circle in Fig. 2(e)), from which lattice fringes are clearly visible. The spacing between neighboring lattice planes is estimated to be ~0.26 nm, which corresponds well to the interplanar distance of the (0001) crystal planes of a hexagonal wurtzite ZnO.

Fig. 3 illustrates the schematic evolution process of the hexagonal nanosheets. It has been reported that the crystallites of polar ZnO can be fabricated usually in an elongated form using the hydrothermal solvents in which the ion OH^- is added [17]. The (0001) and (000$\bar{1}$) faces of ZnO crystal have an equal reticular density but differ in the composition of the outermost atomic layer [18,19]. The outermost layer of the positive monohedron (0001) consists of Zn^{2+} ions and effective charge on this face is close to 2^+. The outermost layer of the negative monohedron (000$\bar{1}$) consists of O^{2-} ions and has a negative charge of the same magnitude. Moreover, the polar growth of ZnO crystal along (0001) direction proceeds through the adsorption of growth units of $[Zn(OH)_4]^{2-}$ onto the (0001) plane of ZnO [20].

In the synthesis systems, the HMT is served as a pH buffer to release OH^- (Eqs. (1) and (2)). The OH^- ions are subsequently reacted with Zn^{2+} to form $[Zn(OH)_4]^{2-}$ (Eq. (3)), which acts as the growth units of ZnO. The ZnO is finally formed *via* a homogeneous precipitation under mild conditions. The overall reaction for the growth of ZnO crystals can be simply formulated as follows:

$$(CH_2)_6N_4 + 6H_2O \leftrightarrow 4NH_3 + 6HCHO \quad (1)$$

$$NH_3 + H_2O \leftrightarrow NH_3 \cdot H_2O \leftrightarrow NH_4^+ + OH^- \quad (2)$$

$$Zn^{2+} + 2OH^- \leftrightarrow Zn(OH)_2\downarrow \overset{2OH^-}{\longleftrightarrow} Zn(OH)_4^{2-} \overset{\Delta}{\longleftrightarrow} ZnO + H_2O \quad (3)$$

However, in the present case, the CTAB was added in the hydrothermal solution. The CTAB is a cation surfactant. When the CTAB dissolves in water, the CTAB ionizes completely, forming CTA^+ ions [21]. At the early stage, $Zn(OH)_4^{2-}$ ions in the solution are combined with the CTA^+ which is released from CTAB to form ion-pairs. The negatively charged ion-pairs are then selectively attached onto the positively charged (0001) surface of ZnO and simultaneously the hydrophobic tails (CTA^+) are aligned into a film. This hydrophobic film inhibits the attachment of growth units of $[Zn(OH)_4]^{2-}$ onto the (0001) face. Accordingly, the intrinsically anisotropic growth of ZnO along the (0001) direction is substantially suppressed and the crystal growth then proceeds sideways, which results in the formation of solid hexagonal ZnO crystals with low aspect ratio at last.

To gain insight into the performances of hexagonal ZnO nanosheets, we further investigate their gas-sensing properties. Fig. 4(a) shows the gas-sensing response of the nanosheets at different working temperatures ranging from 200 to 500 °C under the formaldehyde concentration of 50 ppm. Obviously, the gas response increases to the maximum value of 37.8 at a temperature as low as 350 °C, and gradually decreased with further increasing temperature. Therefore, the optimal working temperature is determined to be 350 °C for further gas-sensing measurements. Response and recovery times are also important for a gas sensor. Fig. 4(b) shows the response and recovery time of the sensor made of the ultrathin ZnO nanosheets to formaldehyde of 50 ppm, which is measured at the optimum temperature of 350 °C. The results indicate that the ZnO sensor shows a fast response–recovery process, and the response and recovery time is estimated to be about 9 and 11 s, respectively.

It is known that the oxygen molecule can capture free electrons from the ZnO nanosheets once they are exposed in air, forming the chemisorbed oxygen species such as O_2^-, O^{2-}, and O^-, which hence results in a high resistance state [10,13]. The absorbed O can induce a depletion layer, bending the surface bands and therefore increasing the energy barrier (*i.e.*, resistance) of the gas sensors. Once the reductive gas is introduced, its molecules react with the chemisorbed oxygen species on the ZnO surface, which releases the trapped electrons back to the conduction band of ZnO. This process can dramatically increase electron concentration in the ZnO sensors and hence enhance its conductivity. As aforementioned, the response of the metal-oxide gas sensors relies largely on the size and dimension of the sensing materials and those materials with a size close to the Debye length can often exhibit excellent sensing responses, holding thereby substantial potentials for detecting gas even at ppm level. Such enhancement of sensing response becomes pronounced as size of nanostructures approaches the threshold value of 15 nm, the Debye length ($2L_D$, which is about 15 nm at 325 °C for ZnO [16]) based on the grain control model. In this study, the prepared nanosheets have a thickness of 17 nm, which means that the entire nanosheets are electron depleted in air, resulting in the maximum resistance. Once being exposed to formaldehyde, the previously trapped electrons by oxygen are retracted

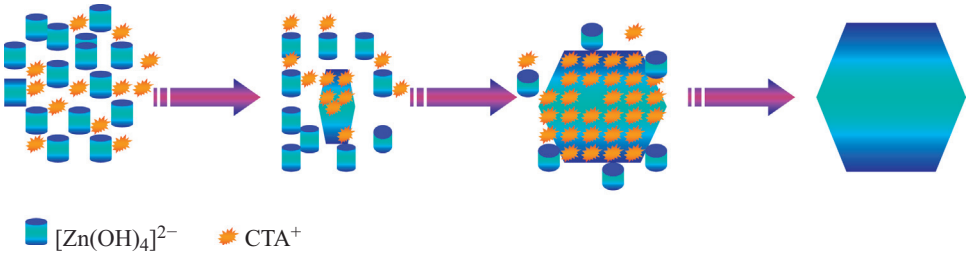

Fig. 3. Schematic plot illustrating the evolution of the ZnO hexagonal nanosheets.

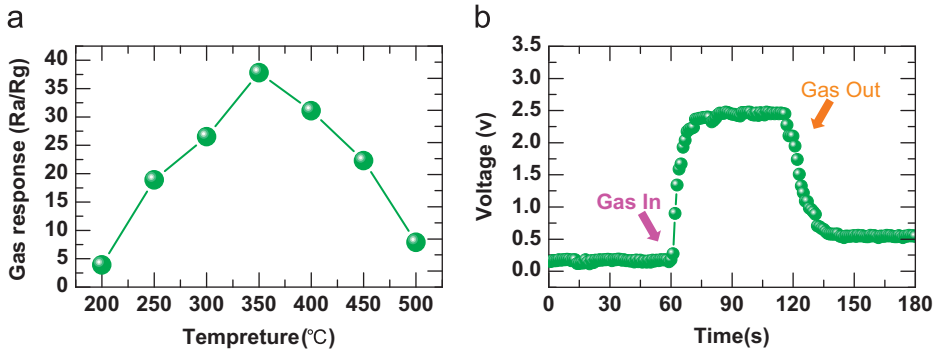

Fig. 4. (a) Sensitivity of the sensor made of ZnO hexagonal nanosheets to the formaldehyde of 50 ppm measured at temperatures from 200 to 500 °C. (b) Response and recovery transients of the sensor made of the ZnO hexagonal nanosheets to the formaldehyde of 50 ppm. The measurement temperature is fixed to 350 °C.

to ZnO due to the mutual reaction between formaldehyde and the oxygen species, leading to a sharp decrease of resistance and a substantial resistance variation *i.e.*, the gas-sensing signal is enhanced.

4. Conclusions

We have successfully fabricated the hexagonal ZnO nanosheets with a thickness as thin as 17 nm *via* a simple yet efficient hydrothermal approach. We investigate the role of the additives on the morphology evolution of the nanosheets and examined the gas-sensing properties of the fabricated sensors. We find that the CTAB additives are aligned on the (0001) surface, based upon which a possible growth mechanism is proposed. Further gas-sensing measurements reveal that the sensor made of hexagonal ZnO nanosheets exhibits a gas response of 37.8 and a response and recovery time of 9 and 11 s, respectively, to the formaldehyde gas of 50 ppm at an optimal temperature of 350 °C.

Acknowledgments

This work is supported by the application development plan, a key project in Chongqing (cstc2013yykfB50008).

References

[1] M. Chen, Z.H. Wang, D.M. Han, F.B. Gu, G.S. Guo, Porous ZnO polygonal nanoflakes: synthesis, use in high-sensitivity NO_2 gas sensor, and proposed mechanism of gas sensing, Journal of Physical Chemistry C 115 (2011) 12763–12773.
[2] J.H. Lee, Gas sensors using hierarchical and hollow oxide nanostructures: overview, Sensors and Actuators B 140 (2009) 319–336.
[3] Z. Wang, J. Song, Piezoelectric nanogenerators based on zinc oxide nanowire arrays, Science 312 (2006) 242–246.
[4] Y. Xia, P. Yang, Y. Sun, Y. Wu, B. Mayers, B. Gates, Y. Yin, F. Kim, Y. Yan, One-dimensional nanostructures: synthesis characterization, and applications, Advanced Materials 15 (2003) 353–389.
[5] X. Liu, J. Zhang, L. Wang, T. Yang, X. Guo, S. Wu, S. Wang, 3D hierarchically porous ZnO structures and their functionalization by Au nanoparticles for gas sensors, Journal of Materials Chemistry 21 (2011) 349–356.
[6] P.D. Yang, H.P. Yan, S. Mao, R. Russo, J. Johnson, R. Saykally, N. Morris, J. Pham, R.R. He, H.J. Choi, Controlled growth of ZnO nanowires and their opitical properties, Advanced Functional Materials 12 (2002) 323–331.
[7] Y. Masuda, K. Kato, Aqueous synthesis of ZnO rod arrays for molecular sensor, Crystal Growth and Design 9 (2009) 3083–3088.
[8] P.X. Gao, Y. Ding, W. Mai, W.L. Hughes, C.S. Lao, Z.L. Wang, Conversion of zinc oxide nanobelts into superlattice-structured nanohelices, Science 309 (2005) 1700–1704.
[9] W.W. Guo, T.M. Liu, R. Sun, Y. Chen, W. Zeng, Z.C. Wang, Hollow, porous, and yttrium functionalized ZnO nanospheres with enhanced gas-sensing performances, Sensors and Actuators B: Chemical 173 (2012) 53–62.
[10] W.W. Guo, T.M. Liu, H.J. Zhang, R. Sun, Y. Chen, W. Zeng, Z.C. Wang, Gas-sensing property performance enhancement in ZnO nanostructures by hierarchical morphology, Sensors and Actuators B: Chemical 166–167 (2012) 492–499.
[11] Y.X. Wang, X.Y. Fan, J. Sun, Hydrothermal synthesis of phosphate-mediated ZnO nanosheets, Materials Letters 63 (2009) 350–352.
[12] J.C. Sin, S.M. Lam, K.T. Lee, A.R. Mohamed, Fabrication of erbium-doped spherical-like ZnO hierarchical nanostructures with enhanced visible light-driven photocatalytic activity, Materials Letters 91 (2013) 1–4.
[13] W.W. Guo, T.M. Liu, W. Zeng, D.J. Liu, Y. Chen, W. Zeng, Z.C. Wang, Gas-sensing property improvement of ZnO by hierarchical flower-like architecture, Materials Letters 65 (2011) 3384–3387.
[14] C. Xu, J. Tamaki, N. Miura, N. Yamazoe, Grain size effects on gas sensitivity of porous SnO_2-based elements, Sensors and Actuators B: Chemical 3 (1991) 147–155.
[15] N. Yamazoe, New approaches for improving semiconductor gas sensors, Sensors and Actuators B: Chemical 5 (1991) 7–19.
[16] N. Hongsith, E. Wongrat, T. Kerdcharoen, S. Choopun, Sensor response formula for sensor based on ZnO nanostructures, Sensors and Actuators B: Chemical 144 (2010) 67–72.
[17] Q. Yu, C. Yu, H. Yang, W. Fu, L. Chang, J. Xu, R. Wei, H. Li, H. Zhu, M. Li, G. Zou, Growth of dumbbell-like ZnO microcrystals under mild conditions and their photoluminescence properties, Inorganic Chemistry 46 (2007) 6204–6210.
[18] M. Chen, Z. Wang, D. Han, F. Gu, G. Guo, High-sensitivity NO_2 gas sensors based on flower-like and tube-like ZnO nanomaterials, Sensors and Actuators B: Chemical 157 (2011) 565–574.
[19] P. Liu, Y. Siao, Ab initio study on preferred growth of ZnO, Scripta Materialia 64 (2011) 483–485.
[20] Y. Zeng, T. Zhang, M. Yuan, M. Kang, G. Lua, R. Wang, H. Fan, Y. He, H. Yang, Growth and selective acetone detection based on ZnO nanorod arrays, Sensors and Actuators B 143 (2009) 93–98.
[21] M. Zhao, D.P. Wu, J.L. Chang, Z.Y. Bai, K. Jiang, Synthesis of cup-like ZnO microcrystals via a CTAB-assisted hydrothermal route, Materials Chemistry and Physics 117 (2009) 422–424.